LECTURE 11: THE MEASUREMENT OF POWER SPECTRUM MULTIPOLES

GONG-BO ZHAO

Abstract. This lecture explains how power-spectrum multipoles are measured in a realistic galaxy survey. We keep the compact 2025 derivations intact, then extend them in the more explanatory 2026 style by adding shell-averaged estimators, simple linear-theory examples, cross-power spectrum multipoles, the connection to configuration space, and the role of BAO reconstruction in pre- and post-reconstruction measurements.

Learning goals

After this lecture, students should be able to:

- write down the Yamamoto and FFT-based estimators for $P_\ell(k)$;
- derive the linear-theory monopole, quadrupole, and hexadecapole for auto- and cross-power spectra;
- explain how shot noise, shell averaging, and the survey window enter a practical measurement;
- connect $P_\ell(k)$ to $\xi_\ell(s)$ through spherical Bessel transforms;
- outline how BAO reconstruction changes the field that is used to measure multipoles.

1. Measurement of power spectrum multipoles

$$\begin{aligned} x &= \chi\cos\delta\cos\alpha \\ y &= \chi\cos\delta\sin\alpha \\ z &= \chi\sin\delta \end{aligned} \tag{1}$$

The Yamamoto estimator,

$$\hat{P}_\ell(k) = \frac{(2\ell+1)}{I}\int\frac{d\Omega_k}{4\pi}\left[\int d\mathbf{r}_1\int d\mathbf{r}_2 F(\mathbf{r}_1)\,F(\mathbf{r}_2)\times e^{i\mathbf{k}\cdot(\mathbf{r}_1-\mathbf{r}_2)}\mathcal{L}_\ell\left(\hat{\mathbf{k}}\cdot\hat{\mathbf{r}}_h\right) - P_\ell^{\rm noise}(\mathbf{k})\right],$$

$$\hat{P}_\ell^{\rm Yama}(k) = \frac{(2\ell+1)}{I}\int\frac{d\Omega_k}{4\pi}\left[\int d\mathbf{r}_1 F(\mathbf{r}_1)\,e^{i\mathbf{k}\cdot\mathbf{r}_1}\times\int d\mathbf{r}_2 F(\mathbf{r}_2)\,e^{-i\mathbf{k}\cdot\mathbf{r}_2}\mathcal{L}_\ell\left(\hat{\mathbf{k}}\cdot\hat{\mathbf{r}}_2\right) - P_\ell^{\rm noise}(\mathbf{k})\right],$$

which can not be evaluated using FFTs.

One solution is the following [1],

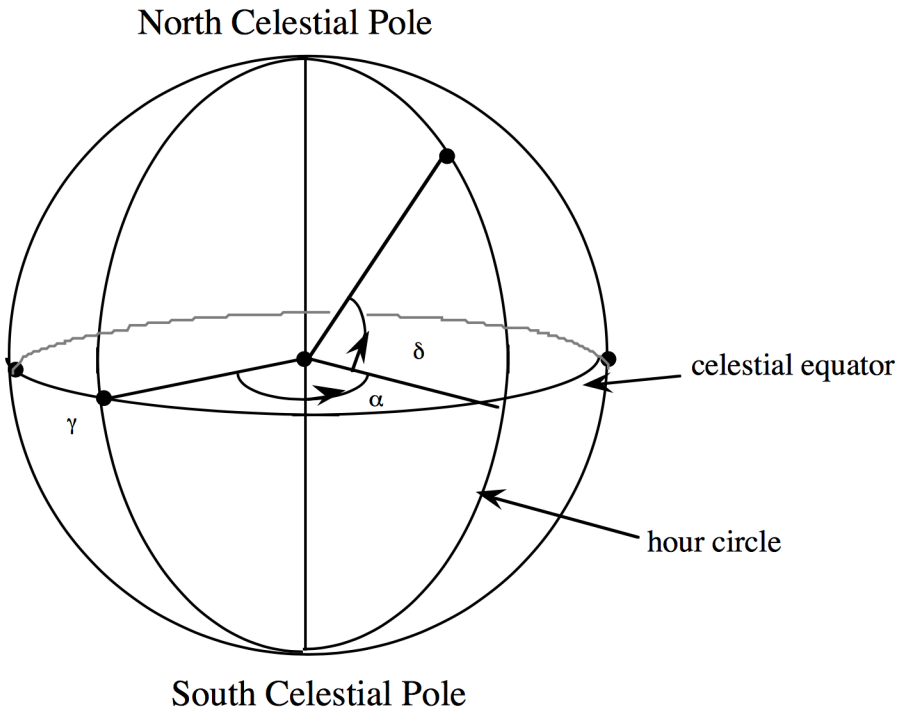

$$A_n(\mathbf{k}) = \int d\mathbf{r}(\hat{\mathbf{k}}\cdot\hat{\mathbf{r}})^n F(\mathbf{r}) e^{i\mathbf{k}\cdot\mathbf{r}} \tag{2}$$

$$\begin{aligned}
\hat{P}_0{}^{\rm Yama}(k) &= \frac{1}{I}\int \frac{d\Omega_k}{4\pi}\left[A_0(\mathbf{k})A_0^*(\mathbf{k})\right] - P_0{}^{\rm noise} \\
\hat{P}_2{}^{\rm Yama}(k) &= \frac{5}{2I}\int \frac{d\Omega_k}{4\pi} A_0(\mathbf{k})\left[3A_2^*(\mathbf{k}) - A_0^*(\mathbf{k})\right] \\
\hat{P}_4{}^{\rm Yama}(k) &= \frac{9}{8I}\int \frac{d\Omega_k}{4\pi} A_0(\mathbf{k})\left[35A_4^*(\mathbf{k}) - 30A_2^*(\mathbf{k}) + 3A_0^*(\mathbf{k})\right]
\end{aligned} \tag{3}$$

$$\hat{\mathbf{k}}\cdot\hat{\mathbf{r}} = \frac{k_x r_x + k_y r_y + k_z r_z}{kr} \tag{4}$$

$$\begin{aligned}
A_2(\mathbf{k}) =& \frac{1}{k^2}\left\{k_x^2 B_{xx}(\mathbf{k}) + k_y^2 B_{yy}(\mathbf{k}) + k_z^2 B_{zz}(\mathbf{k})\right. \\
&\left. + 2\left[k_x k_y B_{xy}(\mathbf{k}) + k_x k_z B_{xz}(\mathbf{k}) + k_y k_z B_{yz}(\mathbf{k})\right]\right\}
\end{aligned} \tag{5}$$

$$B_{ij}(\mathbf{k}) \equiv \int d\mathbf{r} \frac{r_i r_j}{r^2} F(\mathbf{r}) e^{i\mathbf{k}\cdot\mathbf{r}} \tag{6}$$

$$\begin{aligned} A_4(\mathbf{k}) =& \frac{1}{k^4} \left\{ k_x^4 C_{xxx} + k_y^4 C_{yyy} + k_z^4 C_{zzz} \right. \\ &+ 4 \left[k_x^3 k_y C_{xxy} + k_x^3 k_z C_{xxz} + k_y^3 k_x C_{yyx} \right. \\ &+ 4_y^3 k_z C_{yyz} + k_z^3 k_z C_{zzx} + k_z^3 k_y C_{zzy}] \\ &+ 6 \left[k_x^2 k_y^2 C_{xyy} + k_x^2 k_z^2 C_{xzz} + k_y^2 k_z C_{yzz} \right] \\ &\left. + 12 k_x k_y k_z \left[k_x C_{xyz} + k_y C_{yxz} + k_z C_{zxy} \right] \right\} \end{aligned} \tag{7}$$

$$C_{ijl}(\mathbf{k}) \equiv \int d\mathbf{r} \frac{r_i^2 r_j r_l}{r^4} F(\mathbf{r}) e^{i\mathbf{k}\cdot\mathbf{r}} \tag{8}$$

This works, but not efficient. A better way is using the addition theorem [2],

$$\mathcal{L}_\ell \left(\hat{\mathbf{r}}_1 \cdot \hat{\mathbf{r}}_2 \right) = \frac{4\pi}{2\ell + 1} \sum_{m=-\ell}^{\ell} Y_{\ell m} \left(\hat{\mathbf{r}}_1 \right) Y_{\ell m}^{\star} \left(\hat{\mathbf{r}}_2 \right) \tag{9}$$

which is a generalisation of the well-known formula below,

$$\begin{aligned} \sin(x+y) &= \sin(x)\cos(y) + \cos(x)\sin(y) \\ \cos(x+y) &= \cos(x)\cos(y) - \sin(x)\sin(y) \end{aligned} \tag{10}$$

Now,

$$\widehat{P}_\ell(k) = \frac{2\ell + 1}{I} \int \frac{\mathrm{d}\Omega_k}{4\pi} F_0(\mathbf{k}) F_\ell(-\mathbf{k}) \tag{11}$$

$$\begin{aligned} F_\ell(\mathbf{k}) &\equiv \int \mathrm{d}\mathbf{r} F(\mathbf{r}) e^{i\mathbf{k}\cdot\mathbf{r}} \mathcal{L}_\ell(\hat{\mathbf{k}} \cdot \hat{\mathbf{r}}) \\ &= \frac{4\pi}{2\ell + 1} \sum_{m=-\ell}^{\ell} Y_{\ell m}(\hat{\mathbf{k}}) \int \mathrm{d}\mathbf{r} F(\mathbf{r}) Y_{\ell m}^*(\hat{\mathbf{r}}) e^{i\mathbf{k}\cdot\mathbf{r}} \end{aligned} \tag{12}$$

where

$$Y_{\ell m}(\theta, \phi) \equiv \begin{cases} \sqrt{\frac{2\ell+1}{2\pi} \frac{(\ell-m)!}{(\ell+m)!}} \mathcal{L}_\ell^m(\cos\theta) \cos m\phi & m > 0 \\ \sqrt{\frac{2\ell+1}{4\pi}} \mathcal{L}_\ell^m(\cos\theta) & m = 0 \\ \sqrt{\frac{2\ell+1}{2\pi} \frac{(\ell-|m|)!}{(\ell+|m|)!}} \mathcal{L}_\ell^{|m|}(\cos\theta) \sin|m|\phi & m < 0 \end{cases} \tag{13}$$

The equations above are the compact derivation kept from the 2025 notes. The rest of this lecture extends them in the more explanatory 2026 style.

1.1. **Useful definitions and shell averages.** The estimator above measures the multipoles of the anisotropic power spectrum,

$$P(k,\mu)=\sum_{\ell=0}^{\infty}P_\ell(k)\mathcal{L}_\ell(\mu),\qquad P_\ell(k)=\frac{2\ell+1}{2}\int_{-1}^{1}d\mu\,P(k,\mu)\mathcal{L}_\ell(\mu), \tag{14}$$

where $\mu\equiv\hat{\mathbf{k}}\cdot\hat{\mathbf{n}}$. For an auto-power spectrum in the distant-observer limit only even multipoles survive. In practice, for a galaxy survey one usually starts from the weighted overdensity field [3]

$$F(\mathbf{r})=w(\mathbf{r})\left[n_g(\mathbf{r})-\alpha n_s(\mathbf{r})\right], \tag{15}$$

where n_g and n_s are the galaxy and random catalogues, $w(\mathbf{r})$ can include FKP and observational weights, and α fixes the overall normalisation of the random catalogue. A common choice is

$$I=\int d\mathbf{r}\;\left[\bar{n}(\mathbf{r})w(\mathbf{r})\right]^2. \tag{16}$$

The shell-averaged estimator used in practice is

$$\hat{P}_\ell(k_i)=\frac{2\ell+1}{IN_i}\sum_{\mathbf{k}\in k_i}\mathrm{Re}\left[F_0(\mathbf{k})F_\ell(-\mathbf{k})\right]-P_\ell^{\mathrm{noise}}, \tag{17}$$

where the sum runs over all Fourier modes in the bin $k_i-\Delta k/2\le|\mathbf{k}|<k_i+\Delta k/2$ and N_i is the number of modes in that bin. For the standard Poisson model, the shot-noise term mainly affects the monopole, while $P_2^{\mathrm{noise}}=P_4^{\mathrm{noise}}=0$.

Useful identities are

$$\mu^0=\mathcal{L}_0(\mu),\qquad \mu^2=\frac{1}{3}\mathcal{L}_0(\mu)+\frac{2}{3}\mathcal{L}_2(\mu),\qquad \mu^4=\frac{1}{5}\mathcal{L}_0(\mu)+\frac{4}{7}\mathcal{L}_2(\mu)+\frac{8}{35}\mathcal{L}_4(\mu). \tag{18}$$

These identities are often the fastest way to read off the multipoles of any model of the form $A+B\mu^2+C\mu^4$.

1.2. **Simple examples. Example 1: isotropic clustering in real space.** If $P(k,\mu)=P_r(k)$, then

$$P_0(k)=P_r(k),\qquad P_{\ell>0}(k)=0. \tag{19}$$

Thus any non-zero quadrupole or hexadecapole is a direct signature of anisotropy.

Example 2: linear Kaiser redshift-space distortions. In linear theory [4]

$$P^s(k,\mu) = \left(b + f\mu^2\right)^2 P_m(k) = \left[b^2 + 2bf\mu^2 + f^2\mu^4\right] P_m(k). \tag{20}$$

Using the identities above,

$$\begin{aligned} P_0(k) &= \left(b^2 + \frac{2}{3}bf + \frac{1}{5}f^2\right) P_m(k), \\ P_2(k) &= \left(\frac{4}{3}bf + \frac{4}{7}f^2\right) P_m(k), \\ P_4(k) &= \frac{8}{35}f^2 P_m(k). \end{aligned} \tag{21}$$

Therefore P_2 and P_4 vanish when $f = 0$, and the relative size of these multipoles provides a direct measurement of the growth rate.

Writing $\beta \equiv f/b$, the same result becomes

$$\begin{aligned} P_0(k) &= b^2\left(1 + \frac{2}{3}\beta + \frac{1}{5}\beta^2\right) P_m(k), \\ P_2(k) &= b^2\left(\frac{4}{3}\beta + \frac{4}{7}\beta^2\right) P_m(k), \\ P_4(k) &= b^2\frac{8}{35}\beta^2 P_m(k). \end{aligned} \tag{22}$$

1.3. **Cross-power spectrum multipoles.** For two different tracers A and B we define

$$F^A(\mathbf{r}) = w_A(\mathbf{r})\left[n_A(\mathbf{r}) - \alpha_A n_{s,A}(\mathbf{r})\right], \qquad F^B(\mathbf{r}) = w_B(\mathbf{r})\left[n_B(\mathbf{r}) - \alpha_B n_{s,B}(\mathbf{r})\right]. \tag{23}$$

A convenient cross-normalisation is

$$I_{AB} = \int d\mathbf{r}\, \bar{n}_A(\mathbf{r})\bar{n}_B(\mathbf{r}) w_A(\mathbf{r}) w_B(\mathbf{r}), \tag{24}$$

although in the literature one also finds closely related conventions. The natural generalisation of the FFT estimator is

$$\hat{P}_\ell^{AB}(k) = \frac{2\ell+1}{2I_{AB}} \int \frac{d\Omega_k}{4\pi}\left[F_0^A(\mathbf{k})F_\ell^B(-\mathbf{k}) + F_0^B(\mathbf{k})F_\ell^A(-\mathbf{k})\right] - P^{AB}_{\ell,\mathrm{noise}}. \tag{25}$$

The symmetrised form is convenient because it is manifestly real after shell averaging. For independent tracers one usually has $P^{AB}_{\ell,\mathrm{noise}} = 0$. If the two samples overlap, a cross-shot-noise contribution can appear, usually dominated by the monopole.

In linear theory the redshift-space cross-power spectrum is

$$P^{AB}(k,\mu) = \left(b_A + f\mu^2\right)\left(b_B + f\mu^2\right) P_m(k). \tag{26}$$

Therefore

$$
\begin{aligned}
P_0^{AB}(k) &= \left(b_A b_B + \frac{1}{3} f(b_A + b_B) + \frac{1}{5} f^2\right) P_m(k), \\
P_2^{AB}(k) &= \left(\frac{2}{3} f(b_A + b_B) + \frac{4}{7} f^2\right) P_m(k), \\
P_4^{AB}(k) &= \frac{8}{35} f^2 P_m(k).
\end{aligned} \tag{27}
$$

Setting $A = B$ reproduces the auto-spectrum result above. In the distant-observer limit these expressions are even in μ, so only even multipoles are present. Odd multipoles can arise once wide-angle, relativistic, or selection effects are included, and cross-spectra are often the cleanest place to look for them.

1.4. **BAO reconstruction and post-reconstruction multipoles.** Non-linear bulk flows broaden the acoustic peak in configuration space and damp the BAO wiggles in Fourier space. BAO reconstruction uses the large-scale density field to estimate these displacements and move galaxies and randoms part of the way back toward their initial positions [5, 6, 7, 8].

A standard first step is to smooth the observed density field with a Gaussian kernel,

$$
\delta_{\rm sm}(\mathbf{k}) = S(k)\delta_g^s(\mathbf{k}), \qquad S(k) = \exp\left(-\frac{k^2\Sigma_{\rm sm}^2}{2}\right), \tag{28}
$$

with a typical smoothing scale $\Sigma_{\rm sm} \sim 10$–$20\,h^{-1}$Mpc. In the simplest Zel'dovich approximation one estimates the displacement from

$$
\mathbf{\Psi}(\mathbf{k}) = -i\frac{\mathbf{k}}{k^2}\frac{\delta_{\rm sm}(\mathbf{k})}{b}. \tag{29}
$$

If the input field is in redshift space, a common approximation is

$$
\mathbf{\Psi}^s(\mathbf{k}) = -i\frac{\mathbf{k}}{k^2}\frac{\delta_{\rm sm}^s(\mathbf{k})}{b(1+\beta\mu^2)}, \qquad \beta \equiv \frac{f}{b}, \tag{30}
$$

while an iterative first-step estimate can be written as [7]

$$
\delta_{\rm est}^{(1)}(\mathbf{k}) = \frac{\delta_g^s(\mathbf{k})}{b}\left(1 - \frac{\beta}{1+\beta}\mu^2\right). \tag{31}
$$

This makes explicit that reconstruction is trying to infer a smoothed real-space density field from the observed redshift-space one.

The displaced and shifted number-density fields are then built from galaxies and randoms moved backward by the estimated large-scale flow. In compact notation,

$$
F^{\rm rec}(\mathbf{r}) = w(\mathbf{r})\left[n_d^{\rm disp}(\mathbf{r}) - \alpha n_s^{\rm shift}(\mathbf{r})\right], \tag{32}
$$

and the reconstructed density contrast is often written as

$$
\delta_{\rm rec}(\mathbf{r}) = \delta_d(\mathbf{r}) - \delta_s(\mathbf{r}). \tag{33}
$$

Because the reconstructed field has exactly the same form as the pre-reconstruction field, the same FFT estimator may be used again:

$$\hat{P}_\ell^{\rm rec}(k_i) = \frac{2\ell+1}{I_{\rm rec} N_i} \sum_{\mathbf{k}\in k_i} {\rm Re}\left[F_0^{\rm rec}(\mathbf{k}) F_\ell^{\rm rec}(-\mathbf{k})\right] - P_{\ell,{\rm noise}}^{\rm rec}. \tag{34}$$

The main physical effect is that reconstruction reduces the BAO damping scales. Schematically, the wiggle part of the power spectrum changes from

$$P_{\rm wig}^{\rm pre}(k,\mu) \propto \exp\left[-\frac{k^2}{2}\left((1-\mu^2)\Sigma_\perp^2 + \mu^2\Sigma_\parallel^2\right)\right] \tag{35}$$

to

$$P_{\rm wig}^{\rm post}(k,\mu) \propto \exp\left[-\frac{k^2}{2}\left((1-\mu^2)\Sigma_{\perp,{\rm rec}}^2 + \mu^2\Sigma_{\parallel,{\rm rec}}^2\right)\right], \tag{36}$$

with $\Sigma_{\perp,{\rm rec}} < \Sigma_\perp$ and $\Sigma_{\parallel,{\rm rec}} < \Sigma_\parallel$. The acoustic wiggles therefore become sharper, and in configuration space the BAO peak becomes narrower and higher.

Two conventions are common in redshift-space reconstruction. In an isotropic convention (often called *Rec-Iso*), the large-scale Kaiser anisotropy is partly removed from the reconstructed field, so the post-reconstruction quadrupole is small. In a symmetric convention (often called *Rec-Sym*), the large-scale RSD signal is kept, so post-reconstruction monopole and quadrupole can both be modeled and fitted. This matters directly for lecture 11, because the estimator for $P_\ell(k)$ is the same in both cases, but the expected size of the post-reconstruction higher multipoles is not.

1.5. **A practical workflow.** A realistic anisotropic clustering pipeline usually follows these steps:

(1) build the weighted galaxy and random catalogues and convert (α, δ, z) to Cartesian coordinates;
(2) measure pre-reconstruction multipoles P_0, P_2, and usually P_4;
(3) estimate the large-scale displacement field from a smoothed density field and construct the displaced and shifted catalogues;
(4) re-measure post-reconstruction multipoles with the same FFT machinery;
(5) convolve the theory with the survey window and fit either a BAO-only model or a combined BAO+RSD model.

The important practical point is that reconstruction is inserted between two measurements of the same object: before reconstruction one measures multipoles from the observed field, while after reconstruction one measures the multipoles of the displaced-minus-shifted field. This is why the estimator developed in this lecture is used both before and after reconstruction.

1.6. **Practical remarks for FFT-based measurements.** There are two equivalent ways to reduce the line-of-sight dependence to FFTs. The Cartesian decomposition above writes everything in terms of B_{ij} and C_{ijl} fields. The spherical-harmonic form writes

$$D_{\ell m}(\mathbf{k}) \equiv \int d\mathbf{r}\, F(\mathbf{r}) Y^*_{\ell m}(\hat{\mathbf{r}}) e^{i\mathbf{k}\cdot\mathbf{r}}, \tag{37}$$

so that

$$F_\ell(\mathbf{k}) = \frac{4\pi}{2\ell+1} \sum_{m=-\ell}^{\ell} Y_{\ell m}(\hat{\mathbf{k}}) D_{\ell m}(\mathbf{k}). \tag{38}$$

For $\ell = 0, 2, 4$, this requires $1 + 5 + 9 = 15$ FFTs rather than the $1 + 6 + 15 = 22$ FFTs of the direct Cartesian expansion, which is why the spherical-harmonic implementation is usually preferred.

When measuring $P_\ell(k)$ numerically, several practical issues matter. First, the density field must be painted on a grid. The mass-assignment window and aliasing should be corrected, or at least controlled, for example by deconvolving the assignment window and using interlacing. Second, the theory must be convolved with the survey window. Schematically,

$$\langle \hat{P}_\ell(k) \rangle = \sum_{\ell'} \int dq\, q^2\, W_{\ell\ell'}(k, q)\, P_{\ell'}(q), \tag{39}$$

so the observed monopole receives contributions from the true quadrupole and hexadecapole, and vice versa. Third, the integral constraint suppresses power on the very largest scales because the survey mean is estimated from the survey itself. Fourth, cross-spectra are often less sensitive to uncorrelated systematics and can be very useful as null tests, because many additive contaminants do not correlate between two independent tracers.

1.7. **Connection to configuration-space multipoles.** The power spectrum and correlation function multipoles carry the same information. They are related by spherical Bessel transforms,

$$\begin{aligned} \xi_\ell(s) &= i^\ell \int \frac{k^2 dk}{2\pi^2} P_\ell(k) j_\ell(ks), \\ P_\ell(k) &= 4\pi(-i)^\ell \int s^2 ds\, \xi_\ell(s) j_\ell(ks). \end{aligned} \tag{40}$$

This relation is useful in two ways. First, it gives a direct cross-check between a power-spectrum pipeline and a correlation-function pipeline. Second, it explains why the same physical effects, such as redshift-space distortions, wide-angle corrections, and the survey window, can be described either in Fourier space or in configuration space.

Summary

The main lesson of this lecture is that measuring power-spectrum multipoles is conceptually simple but technically subtle. The line-of-sight dependence makes the estimator anisotropic, the survey window mixes multipoles, and the practical implementation relies

on FFT tricks. Once these ingredients are in place, the same machinery can be used for pre-reconstruction and post-reconstruction analyses, for auto-spectra and cross-spectra, and for direct comparison with configuration-space multipoles.

Suggested reading

- Feldman, Kaiser, and Peacock (1994) for the classic weighted power-spectrum estimator.
- Bianchi et al. (2015) and Hand et al. (2017) for FFT-based line-of-sight-dependent estimators.
- Eisenstein et al. (2007), Padmanabhan et al. (2012), Burden et al. (2014), and White (2015) for BAO reconstruction.
- Dodelson and Schmidt for a broad introduction to large-scale-structure statistics.

Homework

(1) **Kaiser multipoles.** Starting from $P^s(k,\mu) = (b + f\mu^2)^2 P_m(k)$, derive $P_0(k)$, $P_2(k)$, and $P_4(k)$.
(2) **Cross-spectrum multipoles.** Starting from $P^{AB}(k,\mu) = (b_A + f\mu^2)(b_B + f\mu^2)P_m(k)$, derive the expressions for $P_0^{AB}(k)$, $P_2^{AB}(k)$, and $P_4^{AB}(k)$.
(3) **Configuration-space connection.** Use the spherical-Bessel relation between $P_\ell(k)$ and $\xi_\ell(s)$ to show why the same physical anisotropy can be discussed in Fourier space or configuration space.
(4) **BAO reconstruction.** Explain why the reconstructed field is written as $\delta_{\rm rec} = \delta_d - \delta_s$, and describe the qualitative difference between the *Rec-Iso* and *Rec-Sym* conventions.

References

[1] D. Bianchi, H. Gil-Marín, R. Ruggeri and W. J. Percival, "Measuring line-of-sight dependent Fourier-space clustering using FFTs," Mon. Not. Roy. Astron. Soc. **453**, no. 1, L11 (2015) doi:10.1093/mnrasl/slv090 [arXiv:1505.05341 [astro-ph.CO]].
[2] N. Hand, Y. Li, Z. Slepian and U. Seljak, "An optimal FFT-based anisotropic power spectrum estimator," JCAP **1707**, no. 07, 002 (2017) doi:10.1088/1475-7516/2017/07/002 [arXiv:1704.02357 [astro-ph.CO]].
[3] H. A. Feldman, N. Kaiser and J. A. Peacock, "Power-spectrum analysis of three-dimensional redshift surveys," Astrophys. J. **426**, 23 (1994) doi:10.1086/174036.
[4] N. Kaiser, "Clustering in real space and in redshift space," Mon. Not. Roy. Astron. Soc. **227**, 1 (1987) doi:10.1093/mnras/227.1.1.
[5] D. J. Eisenstein, H.-J. Seo, E. Sirko and D. N. Spergel, "Improving cosmological distance measurements by reconstruction of the baryon acoustic peak," Astrophys. J. **664**, 675 (2007) doi:10.1086/518755 [astro-ph/0604362].
[6] N. Padmanabhan *et al.*, "A 2 per cent distance to $z = 0.35$ by reconstructing baryon acoustic oscillations - I. Methods and application to the Sloan Digital Sky Survey," Mon. Not. Roy. Astron. Soc. **427**, 2132 (2012) doi:10.1111/j.1365-2966.2012.21888.x [arXiv:1202.0090 [astro-ph.CO]].
[7] H. J. Burden, W. J. Percival, C. Howlett, M. Manera, A. J. Ross and M. Vargas-Magana, "Efficient reconstruction of linear baryon acoustic oscillations in galaxy surveys," Mon. Not. Roy. Astron. Soc. **445**, 3152 (2014) doi:10.1093/mnras/stu1965 [arXiv:1408.1348 [astro-ph.CO]].
[8] M. White, "Reconstructing baryon oscillations," Mon. Not. Roy. Astron. Soc. **450**, 3822 (2015) doi:10.1093/mnras/stv816 [arXiv:1504.03677 [astro-ph.CO]].